

Geophysical Research Letters

RESEARCH LETTER

10.1029/2020GL092067

Key Points:

- Lightning flashes during Dorian's rapid intensification were larger and more energetic than those during moderate intensification
- As Dorian weakened, lightning flashes were more numerous, but were smaller and less energetic than during intensification
- GLM observations reveal processes that affect hurricane intensity, including barotropic mixing and secondary eyewall formation

Supporting Information:

Supporting Information may be found in the online version of this article.

Correspondence to:

P. Duran,
patrick.t.duran@nasa.gov



Citation:

Duran, P., Schultz, C. J., Bruning, E. C., Stevenson, S. N., PeQueen, D. J., Johnson, N. E., et al. (2021). The evolution of lightning flash density, flash size, and flash energy during Hurricane Dorian's (2019) intensification and weakening. *Geophysical Research Letters*, 48, e2020GL092067. <https://doi.org/10.1029/2020GL092067>

Received 14 DEC 2020
Accepted 25 MAR 2021

© 2021. American Geophysical Union. This article has been contributed to by US Government employees and their work is in the public domain in the USA.

The Evolution of Lightning Flash Density, Flash Size, and Flash Energy During Hurricane Dorian's (2019) Intensification and Weakening

Patrick Duran^{1,2} , Christopher J. Schultz^{1,2} , Eric C. Bruning³ ,
Stephanie N. Stevenson⁴, David J. PeQueen³, Nicholas E. Johnson⁶, Roger E. Allen^{2,5},
Matthew R. Smith^{2,7}, and Frank J. LaFontaine^{2,5}

¹NASA Marshall Space Flight Center, Huntsville, AL, USA, ²NASA Short-Term Prediction Research and Transition Center, Huntsville, AL, USA, ³Texas Tech University, Lubbock, TX, USA, ⁴NOAA NWS National Hurricane Center, Miami, FL, USA, ⁵Jacobs Space Exploration Group, Huntsville, AL, USA, ⁶University at Albany, State University of New York, Albany, NY, USA, ⁷University of Alabama in Huntsville, Huntsville, AL, USA

Abstract The two most distinct inner-core lightning outbreaks in Hurricane Dorian (2019) are analyzed using the Geostationary Lightning Mapper (GLM). The first outbreak occurred during Dorian's intensification, including a rapid intensification (RI), and the second occurred during weakening. During RI, inner-core lightning flash density increased as flashes concentrated inside of the radius of maximum wind (RMW). As weakening commenced, numerous flashes still occurred within the RMW, with a flash rate more than three times that during RI—a signal typically associated with strengthening. These flashes, however, were much smaller and less energetic than those during intensification. Evidence is presented that barotropic mixing and secondary eyewall formation increased the number of small, low-energy lightning flashes in the inner core while simultaneously weakening the storm. The results suggest that flash area and energy from GLM could help distinguish between lightning outbreaks that correspond to intensification and those that correspond to weakening.

Plain Language Summary Lightning can be a useful tool for forecasting hurricane intensity. Usually an increase in lightning within the storm means that it is likely to intensify. But sometimes even weakening hurricanes have large lightning outbreaks, so forecasters must carefully look at other data to see what a lightning outbreak really means for a hurricane's intensity. The Geostationary Lightning Mapper (GLM) is a new tool that provides a lot more information about lightning in hurricanes than was previously available. GLM is able to continuously detect the size and energy of lightning flashes, even over the open oceans. Here we show that the lightning flashes in Hurricane Dorian (2019) were larger and more energetic when the storm was intensifying than when it was weakening. We also argue that changes in the location of lightning flashes could help to identify processes that affect a storm's intensity. This information provides clues into how storm structure changes at peak intensity and can potentially help forecasters interpret whether a lightning outbreak signifies storm intensification or weakening.

1. Introduction

Tropical cyclone (TC) intensification is primarily governed by rapidly evolving inner-core convective processes that are difficult to observe. High-resolution, high-frequency observations of TC convection are an essential component of forecasting TC structure and intensity. Continuous monitoring of lightning by ground-based networks such as the National Lightning Detection Network (NLDN) and the World Wide Lightning Location Network (WWLLN) has demonstrated the utility of lightning as a predictor of TC intensity change. Intensifying TCs exhibit a greater number of inner-core (e.g., Molinari et al., 1994; Molinari et al., 1999; Stevenson et al., 2014) and outer rainband (e.g., Bovalo et al., 2014; Stevenson et al., 2016) lightning flashes than TCs that are weakening or maintaining a steady intensity. Inner-core lightning tends to peak prior to the time that a TC reaches its maximum intensity (Abarca et al., 2011; Price et al., 2009), but significant lightning outbreaks also have been observed in weakening storms (Cecil et al., 2010; Jiang & Ramirez, 2013; Xu et al., 2017). These differing results emphasize that caution must be exercised when interpreting lightning outbreaks as a harbinger of TC intensification. Environmental influences might

account for some of this discrepancy, including enhanced convection in some parts of the storm induced by vertical wind shear (Corbosiero & Molinari, 2002, 2003; Fierro et al., 2011). But even steady-state or weakening storms that are not strongly sheared can exhibit inner-core lightning outbreaks. Thus, careful monitoring of the number of lightning flashes can provide valuable insight into TC intensity evolution, but the range of potential outcomes is broad.

The Geostationary Lightning Mapper (GLM) instruments aboard the Geostationary Operational Environmental Satellite (GOES)-16 and GOES-17 satellites provide continuous observations of lightning across most of the Western Hemisphere, including the Atlantic and Eastern Pacific hurricane basins. GLM is a staring optical event detector that measures changes in cloud top radiance produced by lightning (Goodman et al., 2013; Rudlosky et al., 2019). GLM's ability to detect not only flash location but also average flash area (AFA) and total optical energy (TOE) enables the examination of TC lightning from a number of new perspectives. AFA and TOE are physically related to severe storm kinematics and microphysics (Bruning & MacGorman, 2013; Calhoun et al., 2013; Schultz et al., 2015), but their application to TCs has not yet been explored.

In ordinary thunderstorm cells, intense updrafts produce numerous, relatively low-energy lightning flashes, whereas stratiform regions generate fewer but more energetic flashes (Bruning & MacGorman, 2013). In a weak TC, strong, localized inner-core updrafts are often favorable for intensification (Hendricks et al., 2004; Leppert & Petersen, 2010), which means that a large number of low-energy flashes could indicate strengthening. An intense TC, in contrast, is typically characterized by steady ascent spread over a large area of the inner core, with a stratiform region immediately outside of the eyewall. This suggests that intense TCs should have fewer but more intense lightning flashes than weak TCs, even if they are intensifying. Indeed, observations indicate that lightning is less common in strong TCs than in weak TCs (Abarca et al., 2011; Zhang et al., 2015). However, disruptions to the inner-core circulation caused by vertical wind shear (Reasor et al., 2009), secondary eyewall formation (Abarca & Corbosiero, 2011), and barotropic mixing (Guimond et al., 2016) can induce strong, localized updrafts that could increase the number of low-energy flashes. Given that each of these three processes can affect TC intensity in different ways, we hypothesize that monitoring inner-core lightning characteristics can provide further insight into TC intensification.

In this case study of Hurricane Dorian, we will characterize changes in AFA and TOE as the storm reached its peak intensity. We also will demonstrate changes in the spatial structure of lightning at different intensification stages. Some evidence for the role of vertical wind shear, secondary eyewall formation, and barotropic mixing in causing the lightning variability will be presented, along with implications for storm intensity.

2. Data and Methods

Dorian's track, intensity, and radius of maximum wind (RMW) were obtained from the final Automated Tropical Cyclone Forecasting System (ATCF) b-decks and 850–200-mb environmental vertical wind shear from the Statistical Hurricane Intensity Prediction Scheme (SHIPS; DeMaria & Kaplan, 1999) developmental data set.

GLM observations of flash extent density (FED), AFA, and TOE collected throughout Dorian's lifetime were processed using *glmtools* (Bruning et al., 2019). More details on *glmtools*, FED, AFA, and TOE are included in Supplementary Text S1.

In addition to GLM observations, a high-resolution depiction of inner-core processes occurring within Dorian will be presented using visible imagery from GOES-16 processed with the Man computer Interactive Data Access System (McIDAS; Lazzara et al., 1999). These data will be combined with flight-level thermodynamic and radar observations of wind speed and reflectivity from NOAA's P-3 aircraft to analyze physical processes that could contribute to the observed lightning variability.

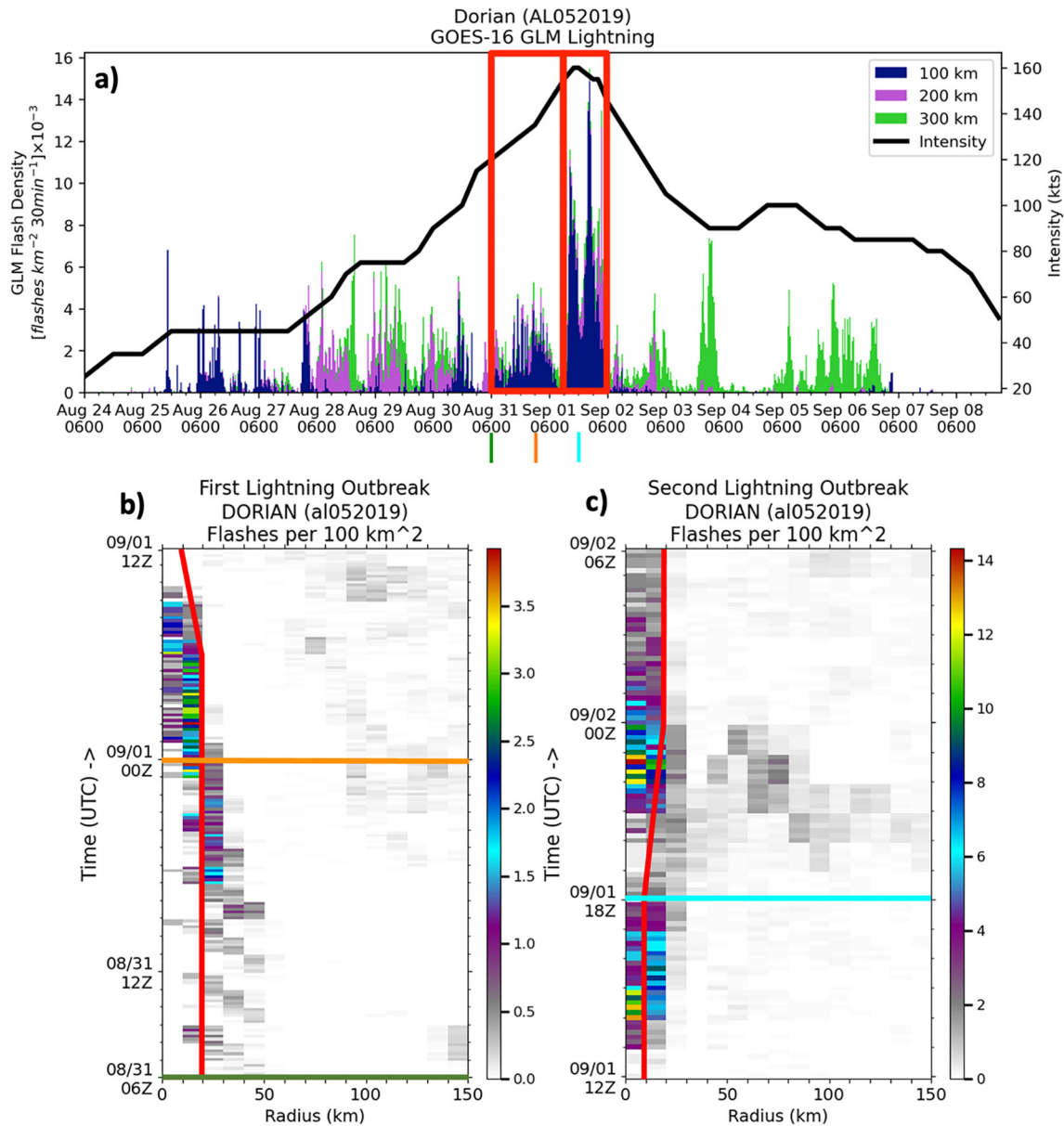


Figure 1. (a) GOES-16 GLM flash count per km^2 in 30-min time periods (left axis) within 100, 200, and 300 km of Hurricane Dorian's (2019) storm center. The black line indicates maximum wind speed (kt; right axis). The two inner-core lightning outbreaks analyzed here are denoted by red boxes. (b), (c) Radius-time diagrams of the number of lightning flashes per 100 km^2 aggregated over 10-min time periods for the (b) first and (c) second lightning outbreaks. Red lines indicate the radius of maximum wind obtained from the Automated Tropical Cyclone Forecasting System b-deck. Dark green, orange, and cyan lines represent the beginning of moderate intensification, rapid intensification, and weakening, respectively.

3. Observations

Hurricane Dorian was an intense hurricane that caused extreme damage and loss of life in the Bahamas. After forming on August 24, 2019, Dorian began a period of intensification on August 27 that culminated with a maximum wind speed of 160 kt shortly before it made landfall in the Abacos on September 1 (Avila et al., 2020). Figure 1a depicts Dorian's intensity and lightning evolution in terms of GLM flash density. A number of inner-core lightning outbreaks (0–100-km; dark blue bars) occurred early in the storm's life (25 August–26 August), followed by large and long-lasting lightning outbreaks within 200 (magenta bars) and 300 (green bars) km of the storm center during the initial intensification (27 August–30 August). Inner-core flash density maximized around the time that Dorian reached its peak intensity. These results are broadly

consistent with previous analyses of flash count: The beginning of intensification corresponded to an increase in outer rainband lightning, and the end of intensification corresponded to an increase in inner-core lightning (e.g., DeMaria et al., 2012; Fierro et al., 2018; Molinari et al., 1999; Stevenson et al., 2016).

The current analysis will focus on the two distinct, long-lived lightning outbreaks that occurred between 06 UTC 31 August and 06 UTC 2 September. The first of these outbreaks (left red box in Figure 1a) occurred while Dorian was intensifying. The second (right red box in Figure 1a) occurred as Dorian reached maximum intensity and began to weaken.

The first lightning outbreak occurred during an intensification period between 06 UTC 31 August and 12 UTC 1 September. This outbreak will be partitioned into two time periods for analysis: One corresponding to moderate intensification (MI) and another corresponding to rapid intensification (RI). Dorian's maximum wind speed increased 15 kt during the 18-h MI period (06 UTC 31 August–00 UTC 1 September) and another 20 kt during the 12-h RI period, which meets the 12-h RI threshold defined by Kaplan et al. (2015).

Figure 1b depicts GLM flash density in radius-time coordinates during the first lightning outbreak. Between 06 and 18 UTC 31 August, four lightning bursts originated near the 50-km radius and propagated inward across the radius of maximum wind (RMW; red line), each over a period of 3 hours. All of these bursts originated just east of Dorian's eye and rotated cyclonically while propagating inward until dissipating to the north or northeast of the eye (Movies S1 and S2). The dissipation of one lightning burst was almost immediately followed by the formation of another at a larger radius to the east of the eye. The final burst formed at 15 UTC and propagated inward until 18 UTC, after which lightning persisted near or just inside the RMW until its abrupt cessation at 09 UTC 1 September. This persistent lightning outbreak within the RMW corresponded to the beginning of RI.

During the first half of RI (00–09 UTC 1 September; Figure 1b), lightning was confined almost entirely inside of the RMW. After a four-hour period (09–13 UTC 1 September) that contained little inner-core lightning during which the RMW contracted from 18.5 to 9.3 km, another inner-core lightning burst erupted at 13 UTC (Figure 1c). The flashes associated with this outbreak straddled the RMW and persisted until Dorian reached its maximum intensity at 18 UTC. This outbreak was more symmetric than the previous, with many flashes occurring in every quadrant (Movie S1).

Figure 2 depicts joint distributions of AFA (km^2) with TOE (femtojoules; left column) and AFA with FED (flashes/ $(2 \text{ km}^2)/(5 \text{ min})$; right column), along with the total number of flashes for each period in the headings. The number of inner-core flashes during MI (1,708) and RI (1,084) yields flash rates of 95 flashes h^{-1} and 90 flashes h^{-1} , respectively. Although flash rates are similar for both phases of intensification, the full distribution of FED reveals changes in the spatial distribution of inner-core lightning that could help distinguish between MI and RI. The FED distribution during MI (Figure 2b) maximizes near 4 flashes/ $(2 \text{ km}^2)/(5 \text{ min})$, whereas during RI (Figure 2d) it maximizes near 9 flashes/ $(2 \text{ km}^2)/(5 \text{ min})$. This near doubling of FED while flash rate remains almost the same can be attributed to a concentration of flashes in a smaller area of the inner core, which would increase the flash density even if the same number of flashes were to occur. This concentration of flashes over a smaller area also can be seen by comparing the MI and RI periods in Figures 1b and 1c. The two phases of intensification also exhibited differing distributions of AFA and TOE. The AFA distribution has a larger spread during MI (Figure 2a) than during RI (Figure 2c), with a broad peak between 700 and 900 km^2 . The RI distribution is narrower and shifted toward larger values, maximizing just above 1,000 km^2 . TOE also shifts toward higher values during RI, peaking at 65 femtojoules, as compared to 45 femtojoules during MI.

As weakening began after 18 UTC 1 September, flash density waned near the RMW and a secondary maximum in lightning density arose near $r = 100 \text{ km}$, propagating inward over the next seven hours before dissipating near the 50-km radius (Figure 1c). This behavior is consistent with a secondary eyewall that was observed during this time in land-based radar reflectivity and wind speed observations from reconnaissance aircraft (not shown). This period was also marked by persistent lightning within an expanding RMW until the outbreak abruptly ended around 06 UTC 2 September (Figure 1c). Akin to the previous day's RI, the inner-core lightning flashes during this phase completely enveloped the eye (see Movie S1).

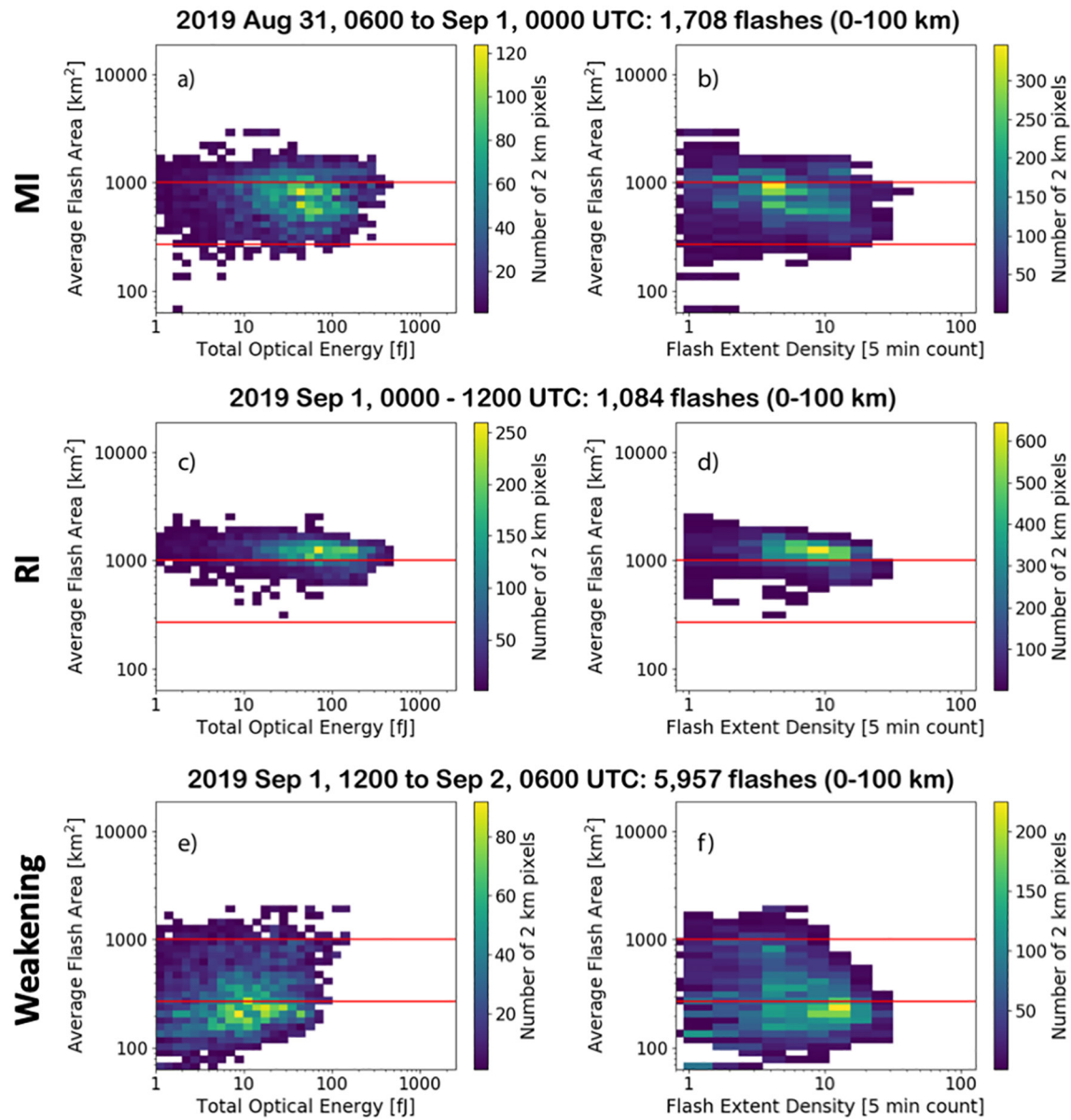


Figure 2. Pixel statistics at GLM group centroids within 100 km of Dorian's center for three time periods: 06 UTC 31 August to 00 UTC 1 September (top row), 00 UTC 1 September to 12 UTC 1 September (middle row), and 12 UTC 1 September to 06 UTC 2 September (bottom row). The bottom red line in each panel denotes the squared GLM group-to-flash clustering distance (16.52 km^2) and the top red line at $1,000 \text{ km}^2$ in each panel is included for reference. Flash extent density is expressed as the number of flashes per five minutes in a 2-km grid cell.

The inner-core joint distributions during Dorian's peak intensity and initial weakening (Figures 2e and 2f) differ considerably from those observed during intensification. The AFA distribution maximizes near 200 km^2 and TOE is shifted toward much smaller values, maximizing near 10 femtojoules. FED (Figure 2f) shifted toward slightly higher values, maximizing near $12 \text{ flashes}/(2 \text{ km}^2)/(5 \text{ min})$. This is consistent with the considerably larger number of flashes during this time, which corresponds to a flash rate of $331 \text{ flashes h}^{-1}$ – more than three times that observed during intensification.

The increase in flash rate and decrease in AFA and TOE as Dorian began to weaken suggests a disruption to the structure of the inner core that led to an increase in the number of strong, localized convective updrafts. Some processes that could have contributed to this disruption are discussed in the next section.

4. Discussion

The evolution of lightning in Hurricane Dorian can be summarized as follows:

1. During MI, lightning bursts erupted outside of the RMW in the downshear-left quadrant and moved cyclonically and radially inward, eventually reaching inside the RMW. Four of these bursts occurred consecutively at three-hour intervals
2. During RI, two outbreaks of persistent lightning occurred. Flashes were concentrated inside of or straddling the RMW and were largely symmetric about the eye
3. Initial weakening saw a decrease in lightning inside of the RMW and an increase in lightning at larger radii. While this secondary maximum in lightning propagated inward, lightning activity within the RMW increased again and persisted even as the storm continued to weaken. Like the RI period, this lightning activity was symmetric about the eye
4. The weakening period exhibited a much greater number of flashes than either period of intensification, but those flashes were smaller and lower-energy

We hypothesize that five processes contributed to the intensity evolution of Hurricane Dorian near its peak intensity: Land interaction, ocean cooling, vertical wind shear, barotropic instability, and secondary eye-wall formation. Although land interaction and ocean cooling probably contributed to Dorian's weakening over the Bahamas (Avila et al., 2020) and may have affected the lightning distribution, the effects of those processes on lightning are not readily apparent in the observations. The latter three processes, however, are readily detectable in the GLM observations, and will be discussed in more detail in the succeeding sections.

4.1. Vertical Wind Shear

The environmental 850–200-mb wind shear during the period of study is depicted in Figure S1. Shear during MI (06 UTC 31 August–00 UTC 1 September) varied between 7 and 10.6 kt with a heading of 108°–140°. Although this is not considered strong shear, the lightning bursts during this time originated in the downshear to downshear-left (east to northeast) part of the storm, which is the expected region of lightning enhancement (Corbosiero & Molinari, 2002, 2003). These bursts rotated cyclonically (Movie S2) as they contracted inward (Figure 1b), with lightning flashes occurring north (upshear-left) of the storm center. The rotation of lightning bursts from the downshear into the upshear quadrants has been linked to TC intensification (Stevenson et al., 2018), consistent with Dorian's intensification during this time. The occurrence of lightning just outside of the RMW, however, is typically associated with weakening (Stevenson et al., 2018). Given that most of the inner-core flashes during this time occurred just outside of the RMW (Figure 1b), a simple analysis of lightning locations relative to the RMW might suggest a weakening trend. This highlights the potential importance of analyzing not just the locations of individual lightning flashes, but also the spatial evolution of lightning bursts. In this case, the inward contraction of each of these bursts could indicate intensification in the presence of vertical wind shear.

During RI between 00 and 18 UTC 1 September, shear decreased from near 12 kt to 5 kt (Figure S1) and lightning flashes occurred within the RMW (Figure 1b) in all quadrants of the storm (Movies S1 and S3). This is consistent with previous work indicating that weak vertical wind shear is conducive to symmetric convection which favors intensification (Frank & Ritchie, 2001). Strong, symmetric eyewall convection induces upper-level outflow that advects ice particles radially outward, creating a region of stratiform precipitation just outside of the eyewall (Black et al., 1996; Marks & Houze, 1987). We hypothesize that this strong outward flow aloft allows for maintenance of a physical connection to continual charge generation processes within the eyewall, much like the front-to-rear convective and stratiform charge structure observed in mesoscale convective systems (Carey et al., 2005; Houze et al., 1996; Schuur et al., 1991; Steiger et al., 2007). Thus, the electric fields will be stronger in and near the eyewall, and when lightning occurs, the flash can tap into additional charge located within the adjacent stratiform region (Reinhart et al., 2014), resulting in larger, more energetic flashes during RI.

After Dorian reached maximum intensity at 18 UTC 1 September, vertical wind shear steadily increased over the next 18 h to near 13 kt. Although 13 kt is still relatively weak shear, this increase in shear could have contributed to Dorian's weakening.

4.2. Barotropic Instability

Satellite imagery revealed the presence of mesovortices in Dorian's eye as the storm reached its maximum intensity on 1 September. The orbit of one of these mesovortices around the center of circulation is documented in Figure S2. As the mesovortex moved along the inner edge of the eyewall, GLM detected lightning flashes (red crosshairs) within the eyewall that rotated around the eye with the cloud swirl. Although the mesovortex indicated by the orange arrows is the most distinct one in the eye at this time, there is evidence of multiple mesovortices within the eye (Movie S3), consistent with previous observational studies (e.g., Kossin et al., 2002).

Low-level mesovortices inject high-entropy air into the low levels of the eyewall (Cram et al., 2007; Schubert et al., 1999) increasing buoyancy and fueling strong updrafts. These updrafts, which can contain vertical velocities exceeding 20 m s^{-1} (Guimond et al., 2016; Hazelton et al., 2017), provide the kinematic and microphysical ingredients necessary for lightning outbreaks characterized by a large number of relatively small and low-energy flashes. Indeed, this time period exhibited the most significant inner-core lightning outbreak observed during the storm's entire life (Figure 1a) and also the smallest and least energetic flashes (Figure 2e). We hypothesize that strong updrafts induced by barotropic mixing result in smaller, less energetic flashes that are entirely contained within the eyewall, similar to those observed in strong, turbulent updrafts in supercells (e.g., Bruning & MacGorman, 2013; Calhoun et al., 2013; Schultz et al., 2015).

Eyewall mesovortices have been associated with both TC intensification and weakening. Mesovortices can enhance convergence in the eyewall (e.g., Guimond et al., 2016) and force highly buoyant low-level air from the eye into the eyewall (e.g., Cram et al., 2007), which feeds strong updrafts and potentially aids intensification. On the other hand, horizontal mixing induced by these mesovortices redistributes vorticity such that it is no longer maximized in the eyewall, but in the eye, a process that weakens the maximum wind speed (Kossin & Eastin, 2001). Dorian's vorticity, wind speed, and reflectivity evolution are depicted in Figure 3 using tail Doppler radar data collected by the NOAA P-3 aircraft. On 31 August (left column), vorticity maximized in the eyewall. This ring-like vorticity pattern is consistent with the presence of barotropic instability (Reasor et al., 2000; Schubert et al., 1999). As Dorian neared its peak intensity on 1 September (center column), four distinct wind speed maxima were located in the eyewall, surrounding the eye (Figure 3e) and the eyewall reflectivity (Figure 3h) was more asymmetric than on the previous day. Although missing data in the eye masks some of the eyewall vorticity structure at this time (Figure 3b), the strong, localized eyewall wind speed maxima imply high-magnitude cyclonic shear located radially inward of the maxima. This, combined with the strong cyclonic rotation of the TC-scale vortex, implies localized vorticity maxima associated with these wind speed maxima, consistent with eyewall mesovortices. By 2 September (right column), the inner-core vorticity profile had evolved toward a monopole maximized at the storm center (Figure 3c). This vorticity evolution, which is consistent with previous studies of eyewall barotropic breakdown, decreases the storm's maximum wind speed (Kossin & Schubert, 2001; Rozoff et al., 2009).

Further evidence of eye–eyewall mixing is seen in flight-level observations collected by the P-3 aircraft (Figure S3). The low-level eye of an intensifying hurricane should warm and dry with time, whereas mixing between the eye and eyewall in a weakening hurricane should cause the eye to become cooler and moister (Cram et al., 2007; Kossin & Eastin, 2001). This evolution was seen in Hurricane Dorian. Each flight leg through Dorian's center on 31 August observed a maximum in both temperature (Figure S3d) and dew point (Figure S3g) in the eye, which corresponded to a broad equivalent potential temperature maximum there (Figure S3a). By 1 September, eye temperature had increased and warmed rapidly between the 1300 and 1,420 UTC flight legs (Figure S3e, blue and orange lines). At the same time, the center of the eye dried considerably, with a dew point minimum at the storm center (Figure S3h). By 2 September (Figure S3, right column), the distinct temperature maximum and dew point minimum near the storm center had disappeared, and equivalent potential temperature gradients near the eye had relaxed.

The evolution described above implies that a sudden outbreak of inner-core lightning in an intense TC could represent the beginning of a barotropic breakdown of the eyewall that marks the end of intensification. We hypothesize that a large number of relatively small, low-energy flashes within the eyewall signals the end of a period of intensification and either the beginning of a period of weakening and/or the

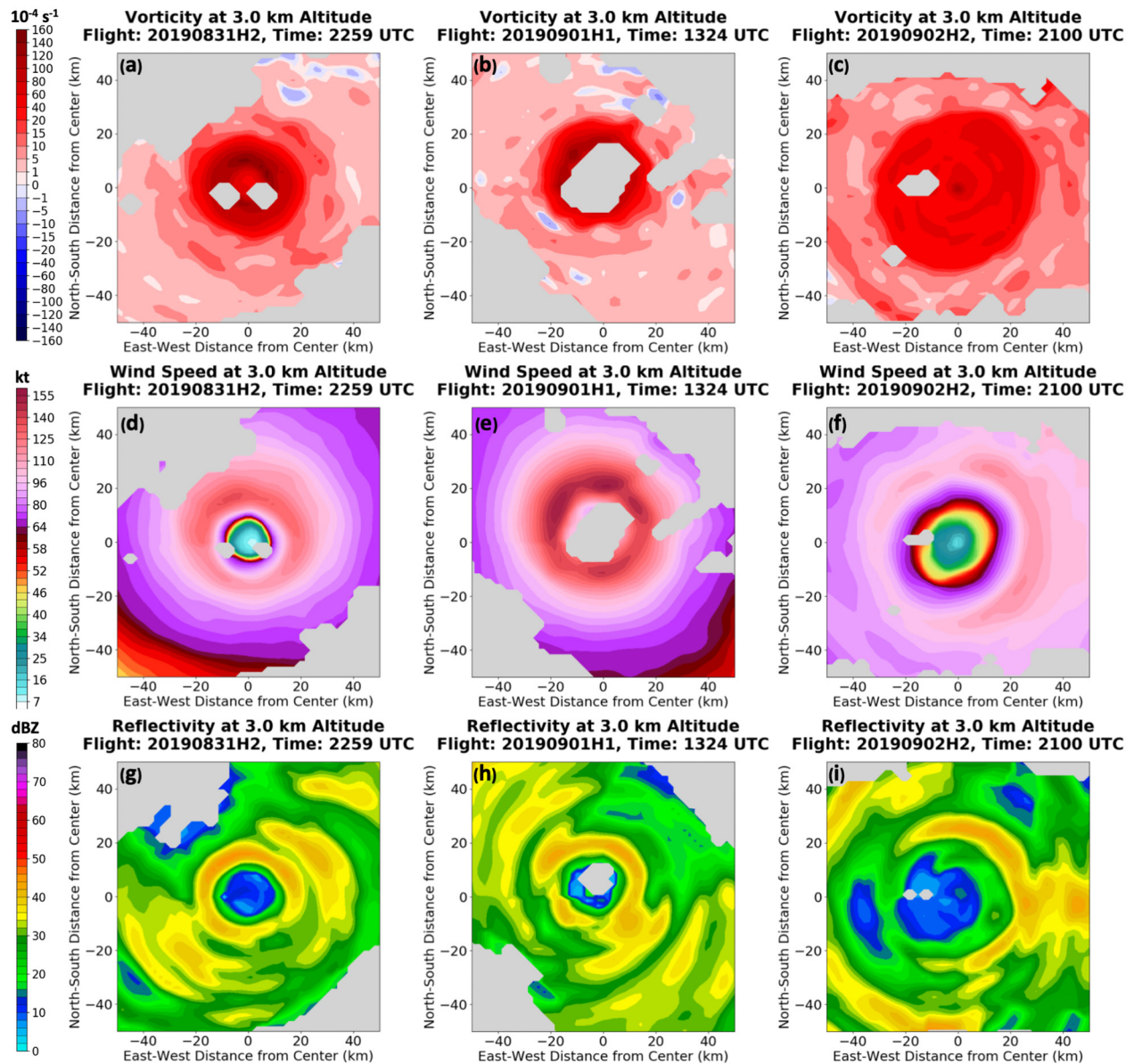


Figure 3. Inner-core vertical vorticity (10^{-4} s^{-1} ; top row), wind speed (kt; middle row), and reflectivity (dBZ; bottom row) observed at 3-km altitude by the NOAA/AOML Hurricane Research Division WP3-D tail Doppler radar for center passes on 31 August (left column), 1 September (center column), and 2 September (right column).

transition of the storm to a steady-state annular hurricane (Knaff et al., 2003). They also could indicate the presence of processes conducive to secondary eyewall formation, which also usually halts intensification.

4.3. Secondary Eyewall Formation

Eyewall mesovortices have been linked to the radiation of vortex Rossby waves (Abarca & Corbosiero, 2011; VRWs Corbosiero et al., 2006). These waves, which propagate both azimuthally and radially outward from the eyewall, deposit momentum at their stagnation radius, which is near three times the radius of maximum winds (Corbosiero et al., 2006; Montgomery & Kallenbach, 1997). The repetitive stagnation of VRWs at this radius can increase the wind speed there and lead to secondary eyewall formation (Abarca & Corbosiero, 2011; Guimond et al., 2020).

Figure 1c depicts a secondary eyewall after Dorian reached maximum intensity at 18 UTC on 1 September. Lightning increased near the 100-km radius and briefly decreased near the RMW, consistent with convective enhancement in a secondary eyewall and suppression near the RMW due to subsidence induced by the new eyewall. As this secondary eyewall contracted inward, however, lightning erupted once again near the RMW as the storm continued to weaken. Given the link between barotropic instability and VRWs, and also the link between VRWs and secondary eyewall formation, we hypothesize that an inner-core lightning outbreak characterized by small and low-energy flashes could be a potential predictor of secondary eyewall formation. Barotropic mixing and a secondary eyewall could act in tandem to weaken a storm even while numerous lightning flashes are occurring near or within the RMW.

Although these results cannot allow a conclusive attribution of the lightning outbreak during Dorian's weakening to any one process, they do suggest that the influence of barotropic instability and eye-eyewall mixing should at least be considered as a possible contributor. An investigation of GLM FED, AFA, and TOE during different intensification phases is currently being undertaken using data from a large number of storms.

5. Conclusions and Future Work

The two most distinct and persistent inner-core lightning outbreaks of Hurricane Dorian's lifetime were analyzed. One outbreak occurred during a period of both moderate and rapid intensification. The second outbreak commenced shortly before the storm reached its maximum intensity and persisted for the first 12 h of weakening. The FED, AFA, and TOE distributions differed considerably between these two outbreaks.

Inner-core lightning flashes during intensification were larger and more energetic than those during weakening. Separately analyzing the first and second parts of the intensification outbreak reveals variability even within this outbreak. The period of moderate intensification was characterized by lightning bursts that arose downshear-left of the storm center and rotated cyclonically inward, crossing the RMW to the left of the shear vector. The lightning outbreak during RI was more axisymmetric, and flashes were contained within or near the RMW. These flashes were also larger and more energetic than those observed during moderate intensification.

A potentially important result of this analysis is that FED, AFA, and TOE could help to distinguish between lightning outbreaks that correspond to intensification and those that represent weakening. The value of these metrics is emphasized by the fact that the lightning flash rate during Dorian's initial weakening was more than triple the rate during rapid intensification. If increasing flash rate is accompanied by decreasing AFA and TOE, this could be a signal that processes are occurring which simultaneously increase the number of lightning flashes and weaken the storm.

Future work will characterize flash area and optical energy in a large number of storms, stratifying by storm intensity, intensification rate, and environmental vertical wind shear. The effect of barotropic mixing on microphysical and kinematic properties relevant to TC electrification also will be analyzed in idealized models.

Data Availability Statement

The GLM and ABI data employed in this paper are publicly available from NOAA CLASS at https://www.avl.class.noaa.gov/saa/products/search?datatype\text{_}family=GRGLMPROD and https://www.avl.class.noaa.gov/saa/products/search?sub\text{_}id=0&datatype\text{_}family=GRABIPRD&submit.x=28&-submit.y=11

References

- Abarca, S. F., & Corbosiero, K. L. (2011). Secondary eyewall formation in WRF simulations of Hurricanes Rita and Katrina (2005). *Geophysical Research Letters*, 38(7), L07802. <https://doi.org/10.1029/2011gl047015>
- Abarca, S. F., Corbosiero, K. L., & Vollaro, D. (2011). The world wide lightning location network and convective activity in tropical cyclones. *Monthly Weather Review*, 139(1), 175–191. <https://doi.org/10.1175/2010MWR3383.1>

Acknowledgments

The authors thank Paul Reasor of NOAA/AOML/Hurricane Research Division for providing the tail Doppler radar data, four reviewers at the National Hurricane Center, and three anonymous reviewers for their helpful comments on the manuscript. Duran, Schultz, Allen, Smith, and LaFontaine are directly supported by Dr. Tsengdar Lee of NASA's Research and Analysis Program, Weather Focus Area, as part of the Short-term Prediction Research and Transition (SPoRT) Center at Marshall Space Flight Center. Bruning and PeQueen are supported by GOES-R Cal/Val award to Texas Tech University under NASA Grant 80NSSC19K1576 and NOAA's JTTI program via CICS-MD award NA14NEWS4320003/66,892-Z7813012.

- Avila, L. A., Stewart, S. R., Berg, R., & Hagen, A. B. (2020). National hurricane center tropical cyclone report: Hurricane Dorian. [https://www.nhc.noaa.gov/data/tcr/AL052019.txt\(_Dorian.pdf](https://www.nhc.noaa.gov/data/tcr/AL052019.txt(_Dorian.pdf)
- Black, M. L., Burpee, R. W., Marks, F. D. (1996). Vertical motion characteristics of tropical cyclones determined with airborne doppler radial velocities. *Journal of Atmospheric Science*, 53(13), 1887–1909. [https://doi.org/10.1175/1520-0469\(1996\)053<1887:vmcotc>2.0.co;2](https://doi.org/10.1175/1520-0469(1996)053<1887:vmcotc>2.0.co;2)
- Bovalo, C., Barthe, C., Yu, N., & Bègue, N. (2014). Lightning activity within tropical cyclones in the south west Indian Ocean. *Journal of Geophysical Research - D: Atmospheres*, 119(13), 8231–8244. <https://doi.org/10.1002/2014JD021651>
- Bruning, E. C., & MacGorman, D. R. (2013). Theory and observations of controls on lightning flash size spectra. *Journal of the Atmospheric Sciences*, 70(12), 4012–4029. <https://doi.org/10.1175/jas-d-12-0289.1>
- Bruning, E. C., Tillier, C. E., Edgington, S. F., Rudlosky, S. D., Zajic, J., Gravelle, C., et al. (2019). Meteorological imagery for the geostationary lightning mapper. *Journal of Geophysical Research - D: Atmospheres*, 124(24), 14285–14309. <https://doi.org/10.1029/2019JD030874>
- Calhoun, K. M., MacGorman, D. R., Ziegler, C. L., & Biggerstaff, M. I. (2013). Evolution of lightning activity and storm charge relative to dual-doppler analysis of a high-precipitation supercell storm. *Monthly Weather Review*, 141(7), 2199–2223. <https://doi.org/10.1175/mwr-d-12-00258.1>
- Carey, L. D., Murphy, M. J., McCormick, T. L., & Demetriades, N. W. S. (2005). Lightning location relative to storm structure in a leading-line, trailing-stratiform mesoscale convective system. *Journal of Geophysical Research*, 110(D3), D03105. <https://doi.org/10.1029/2003jd004371>
- Cecil, D. J., Quinlan, K. R., & Mach, D. M. (2010). Intense convection observed by NASA ER-2 in Hurricane Emily (2005). *Monthly Weather Review*, 138(3), 765–780. <https://doi.org/10.1175/2009mwr3063.1>
- Corbosiero, K. L., & Molinari, J. (2002). The effects of vertical wind shear on the distribution of convection in tropical cyclones. *Monthly Weather Review*, 130(8), 2110–2123. [https://doi.org/10.1175/1520-0493\(2002\)130<2110:TEOVWS>2.0.CO](https://doi.org/10.1175/1520-0493(2002)130<2110:TEOVWS>2.0.CO)
- Corbosiero, K. L., & Molinari, J. (2003). The relationship between storm motion, vertical wind shear, and convective asymmetries in tropical cyclones. *Journal of the Atmospheric Sciences*, 60(2), 366–376. [https://doi.org/10.1175/1520-0469\(2003\)060<0366:TRBSMV>2.0.CO](https://doi.org/10.1175/1520-0469(2003)060<0366:TRBSMV>2.0.CO)
- Corbosiero, K. L., Molinari, J., Ayyer, A. R., & Black, M. L. (2006). The structure and evolution of hurricane Elena (1985). Part II: Convective asymmetries and evidence for vortex rossby waves. *Monthly Weather Review*, 134(11), 3073–3091. <https://doi.org/10.1175/mwr3250.1>
- Cram, T. A., Persing, J., Montgomery, M. T., & Braun, S. A. (2007). A lagrangian trajectory view on transport and mixing processes between the eye, eyewall, and environment using a high-resolution simulation of hurricane Bonnie (1998). *Journal of the Atmospheric Sciences*, 64(6), 1835–1856. <https://doi.org/10.1175/jas3921.1>
- DeMaria, M., DeMaria, R. T., Knaff, J. A., & Molinar, D. (2012). Tropical cyclone lightning and rapid intensity change. *Monthly Weather Review*, 140(6), 1828–1842. <https://doi.org/10.1175/mwr-d-11-00236.1>
- DeMaria, M., & Kaplan, J. (1999). An updated Statistical Hurricane Intensity Prediction Scheme (SHIPS) for the Atlantic and Eastern North Pacific Basins. *Weather and Forecasting*, 14, 12. [https://doi.org/10.1175/1520-0434\(1999\)014<0326:auship>2.0.co;2](https://doi.org/10.1175/1520-0434(1999)014<0326:auship>2.0.co;2)
- Fierro, A. O., Shao, X.-M., Hamlin, T., Reisinger, J. M., & Harlin, J. (2011). Evolution of eyewall convective events as indicated by intracloud and cloud-to-ground lightning activity during the rapid intensification of hurricanes rita and katrina. *Monthly Weather Review*, 139(5), 1492–1504. <https://doi.org/10.1175/2010MWR3532.1>
- Fierro, A. O., Stevenson, S. N., & Rabin, R. M. (2018). Evolution of GLM-observed total lightning in hurricane Maria (2017) during the period of maximum intensity. *Monthly Weather Review*, 146(6), 1641–1666. <https://doi.org/10.1175/mwr-d-18-0066.1>
- Frank, W. M., & Ritchie, E. A. (2001). Effects of vertical wind shear on the intensity and structure of numerically simulated hurricanes. *Monthly Weather Review*, 129(9), 2249–2269. [https://doi.org/10.1175/1520-0493\(2001\)129<2249:evovwso>2.0.co;2](https://doi.org/10.1175/1520-0493(2001)129<2249:evovwso>2.0.co;2)
- Goodman, S. J., Blakeslee, R. J., Koshak, W. J., Mach, D., Bailey, J., Buechler, D., et al. (2013). The GOES-R Geostationary Lightning Mapper (GLM). *Atmospheric Research*, 125–126, 34–49. <https://doi.org/10.1175/j.atmosres.2013.01.006>
- Guimond, S. R., Heymsfield, G. M., Reasor, P. D., & Didlake, A. C. (2016). The rapid intensification of hurricane Karl (2010): New remote sensing observations of convective bursts from the global hawk platform. *Journal of the Atmospheric Sciences*, 73(9), 3617–3639. <https://doi.org/10.1175/jas-d-16-0026.1>
- Guimond, S. R., Reasor, P. D., Heymsfield, G. M., & McLinden, M. M. (2020) The dynamics of vortex rossby waves and secondary eyewall development in hurricane matthew (2016): New insights from radar measurements. *Journal of the Atmospheric Sciences*, 77(7), 2349–2374. [10.1175/JAS-D-19-0284.1](https://doi.org/10.1175/JAS-D-19-0284.1)
- Hazelton, A. T., Rogers, R. F., & Hart, R. E. (2017). Analyzing simulated convective bursts in two atlantic hurricanes. Part I: Burst formation and development. *Monthly Weather Review*, 145(8), 3073–3094. <https://doi.org/10.1175/mwr-d-16-0267.1>
- Hendricks, E. A., Montgomery, M. T., & Davis, C. A. (2004). The role of “vortical” hot towers in the formation of tropical cyclone diana (1984). *Journal of the Atmospheric Sciences*, 61(11), 1209–1232. [https://doi.org/10.1175/1520-0469\(2004\)061<1209:trovht>2.0.co;2](https://doi.org/10.1175/1520-0469(2004)061<1209:trovht>2.0.co;2)
- Houze, R. A., Rutledge, S. A., Biggerstaff, M. I., & Smull, B. F. (1996). Interpretation of doppler weather radar displays of midlatitude mesoscale convective systems. *Bulletin of the American Meteorological Society*, 53(13), 1887–1909
- Jiang, H., & Ramirez, E. M. (2013). Necessary conditions for tropical cyclone rapid intensification as derived from 11 years of trmm data. *Journal of Climate*, 26(17), 6459–6470. <https://doi.org/10.1175/JCLI-D-12-00432.1>
- Kaplan, J., Rozoff, C. M., DeMaria, M., Sampson, C. R., Kossin, J. P., Velden, C. S., et al. (2015). In Evaluating Environmental Impacts on Tropical Cyclone Rapid Intensification Predictability Utilizing Statistical Models. *Weather and Forecasting*, October 30 (pp. 1374–1396). (Publisher: American Meteorological Society Section: Weather and Forecasting)
- Knaff, J. A., Kossin, J. P., & DeMaria, M. (2003). Annular hurricanes. *Weather and Forecasting*, 18(2), 204–223. [https://doi.org/10.1175/1520-0434\(2003\)018<0204:ah>2.0.co;2](https://doi.org/10.1175/1520-0434(2003)018<0204:ah>2.0.co;2)
- Kossin, J. P., & Eastin, M. D. (2001). Two distinct regimes in the kinematic and thermodynamic structure of the hurricane eye and eyewall. *Journal of the Atmospheric Sciences*, 58(9), 1079–1090. [https://doi.org/10.1175/1520-0469\(2001\)058<1079:tdtrict>2.0.co;2](https://doi.org/10.1175/1520-0469(2001)058<1079:tdtrict>2.0.co;2)
- Kossin, J. P., McNoldy, B. D., & Schubert, W. H. (2002). Vortical Swirls in Hurricane Eye Clouds. *Monthly Weather Review*, 130(12), 3144–3149. [https://doi.org/10.1175/1520-0493\(2002\)130<3144:vsihcc>2.0.co;2](https://doi.org/10.1175/1520-0493(2002)130<3144:vsihcc>2.0.co;2)
- Kossin, J. P., & Schubert, W. H. (2001). Mesovortices, polygonal flow patterns, and rapid pressure falls in hurricane-like vortices. *Journal of the Atmospheric Sciences*, 58(15), 2196–2209. [https://doi.org/10.1175/1520-0469\(2001\)058<2196:mpfpar>2.0.co;2](https://doi.org/10.1175/1520-0469(2001)058<2196:mpfpar>2.0.co;2)
- Lazzara, M. A., Benson, J. M., Fox, R. J., Laitsch, D. J., Rueden, J. P., Santek, D. A., et al. (1999). The man computer interactive data access system: 25 years of interactive processing. *Bulletin of the American Meteorological Society*, 80(2), 271–284. [https://doi.org/10.1175/1520-0477\(1999\)080<0271:tmcida>2.0.co;2](https://doi.org/10.1175/1520-0477(1999)080<0271:tmcida>2.0.co;2)
- Leppert, K. D., & Petersen, W. A. (2010). Electrically active hot towers in African easterly waves prior to tropical cyclogenesis. *Monthly Weather Review*, 138(3), 663–687. <https://doi.org/10.1175/2009mwr3048.1>

- Marks, F. D., Houze, R. A. (1987). Inner core structure of hurricane alicia from airborne doppler radar observations. *Journal of the Atmospheric Sciences*, 44(9), 1296–1317. [https://doi.org/10.1175/1520-0469\(1987\)044<1296:icsoha>2.0.co;2](https://doi.org/10.1175/1520-0469(1987)044<1296:icsoha>2.0.co;2)
- Molinari, J., Moore, P., & Idone, V. (1999). Convective structure of hurricanes as revealed by lightning locations. *Monthly Weather Review*, 127(4), 520–534. [https://doi.org/10.1175/1520-0493\(1999\)127<0520:CSOHAR>2.0.CO](https://doi.org/10.1175/1520-0493(1999)127<0520:CSOHAR>2.0.CO)
- Molinari, J., Moore, P. K., Idone, V. P., Henderson, R. W., & Saljoughy, A. B. (1994). Cloud-to-ground lightning in hurricane andrew. *Journal of Geophysical Research*, 99, 16665–16676. <https://doi.org/10.1175/2008WAF2222128.110.1029/94jd00722>
- Montgomery, M. T., & Kallenbach, R. J. (1997). A theory for vortex rossby-waves and its application to spiral bands and intensity changes in hurricanes. *Quarterly Journal of the Royal Meteorological Society*, 123(538), 435–465. <https://doi.org/10.1002/qj.49712353810>
- Price, C., Asfur, M., & Yair, Y. (2009). Maximum hurricane intensity preceded by increase in lightning frequency. *Nature Geoscience*, 2, 329–332. <https://doi.org/10.1038/ngeo477>
- Reasor, P. D., Eastin, M. D., & Gamache, J. F. (2009). Rapidly intensifying hurricane guillermo (1997). Part I: Low-wavenumber structure and evolution. *Monthly Weather Review*, 137(2), 603–631. <https://doi.org/10.1175/2008mwr2487.1>
- Reasor, P. D., Montgomery, M. T., Marks, F. D., Gamache, J. F., & Gamache, J. F. (2000). Low-wavenumber structure and evolution of the hurricane inner core observed by airborne dual-doppler radar. *Monthly Weather Review*, 128(6), 1653–1680. [https://doi.org/10.1175/1520-0493\(2000\)128<1653:lwsao>2.0.co;2](https://doi.org/10.1175/1520-0493(2000)128<1653:lwsao>2.0.co;2)
- Reinhart, B., Fuelberg, H., Blakeslee, R., Mach, D., Heymsfield, A., Bansemir, A., et al. (2014). Understanding the relationships between lightning, cloud microphysics, and airborne radar-derived storm structure during hurricane Karl (2010). *Monthly Weather Review*, 142(2), 590–605. <https://doi.org/10.1175/mwr-d-13-00008.1>
- Rozoff, C. M., Kossin, J. P., Schubert, W. H., & Mulero, P. J. (2009). Internal control of hurricane intensity variability: The dual nature of potential vorticity mixing. *Journal of the Atmospheric Sciences*, 66(1), 133–147. <https://doi.org/10.1175/2008jas2717.1>
- Rudlosky, S. D., Goodman, S. J., Virts, K. S., & Bruning, E. C. (2019). Initial geostationary lightning mapper observations. *Geophysical Research Letters*, 46(2), 1097–1104. <https://doi.org/10.1029/2018gl081052>
- Schubert, W. H., Montgomery, M. T., Taft, R. K., Guinn, T. A., Fulton, S. R., Kossin, J. P., & Edwards, J. P. (1999). Polygonal eyewalls, asymmetric eye contraction, and potential vorticity mixing in hurricanes. *Journal of the Atmospheric Sciences*, 56, 27. [https://doi.org/10.1175/1520-0469\(1999\)056<1197:peaeca>2.0.co;2](https://doi.org/10.1175/1520-0469(1999)056<1197:peaeca>2.0.co;2)
- Schultz, C. J., Carey, L. D., Schultz, E. V., & Blakeslee, R. J. (2015). Insight into the kinematic and microphysical processes that control lightning jumps. *Weather and Forecasting*, 30(6), 1591–1621. <https://doi.org/10.1175/waf-d-14-00147.1>
- Schuur, T. J., Rust, W. D., Smull, B. F., & Marshall, T. C. (1991). Electrical and kinematic structure of the stratiform precipitation region trailing an Oklahoma squall line. *Journal of the Atmospheric Sciences*, 48(6), 825–842. [https://doi.org/10.1175/1520-0469\(1991\)048<0825:eaksot>2.0.co;2](https://doi.org/10.1175/1520-0469(1991)048<0825:eaksot>2.0.co;2)
- Steiger, S. M., Orville, R. E., & Carey, L. D. (2007). Total lightning signatures of thunderstorm intensity over North Texas. Part II: Mesoscale convective systems. *Monthly Weather Review*, 135(10), 3303–3324. <https://doi.org/10.1175/mwr3483.1>
- Stevenson, S. N., Corbosiero, K. L., & Abarca, S. F. (2016). Lightning in eastern north pacific tropical cyclones: A comparison to the North Atlantic. *Monthly Weather Review*, 144(1), 225–239. <https://doi.org/10.1175/MWR-D-15-0276.1>
- Stevenson, S. N., Corbosiero, K. L., DeMaria, M., & Vigh, J. L. (2018). A 10-year survey of tropical cyclone inner-core lightning bursts and their relationship to intensity change. *Weather and Forecasting*, 33(1), 23–36. <https://doi.org/10.1175/waf-d-17-0096.1>
- Stevenson, S. N., Corbosiero, K. L., & Molinari, J. (2014). The convective evolution and rapid intensification of hurricane earl (2010). *Monthly Weather Review*, 142(11), 4364–4380. <https://doi.org/10.1175/MWR-D-14-00078.1>
- Xu, W., Rutledge, S. A., & Zhang, W. (2017). Relationships between total lightning, deep convection, and tropical cyclone intensity change. *Journal of Geophysical Research - D: Atmospheres*, 122(13), 7047–7063. <https://doi.org/10.1002/2017JD027072>
- Zhang, W., Zhang, Y., Zheng, D., Wang, F., & Xu, L. (2015). Relationship between lightning activity and tropical cyclone intensity over the northwest Pacific. *Journal of Geophysical Research - D: Atmospheres*, 120(9), 4072–4089. <https://doi.org/10.1002/2014jd022334>